3D free surface flow simulations based on the integral form of the equations of motion

GIOVANNI CANNATA, CHIARA PETRELLI, LUCA BARSI, FLAMINIA CAMILLI,
FRANCESCO GALLERANO
Department of Civil, Constructional and Environmental Engineering
"Sapienza" University of Rome
Via Eudossiana 18, 00184
ITALY
giovanni.cannata@uniroma1.it   https://www.dicea.uniroma1.it/en/users/giovannicannata

Abstract: This work deals with a novel three-dimensional finite-volume non-hydrostatic shock-capturing model for the simulation of wave transformation processes and wave-structure interaction. The model is based on an integral formulation of the Navier-Stokes equations solved on a coordinate system in which the vertical coordinate is varying in time. A finite-volume shock-capturing numerical technique based on high order WENO reconstructions is adopted in order to discretize the fluid motion equations.

Key-Words: three-dimensional, time-dependent coordinate system, free surface flow, shock-capturing

1 Introduction

The modelling of surface wave transformation processes is crucial when dealing with the simulation of the hydrodynamic phenomena in coastal regions. Three-dimensional equations of motion can be used in order to represent most of these processes. In the most recent 3D models [15], the dynamic pressure is taken into account (free surface fully non-hydrostatic models). In such models, the total pressure is decomposed in its dynamic and hydrostatic parts. The solution of the fluid motion governing equations can be obtained as a succession of two different steps: in the first one, the convective terms are discretised together with those related to the hydrostatic pressure, the bottom slope and the stress term; in the second one, the so-called Poisson equation is solved in order to compute the dynamic pressure. In the firsts free surface fully non-hydrostatic models, Cartesian coordinates were used with proper free tracking technique [4]. By this way, the calculation cells are arbitrarily crossed by the vertical fluxes making it difficult to correctly assign the pressure kinematic condition for the free surface elevation. As a consequence, spurious oscillations are present in the numerical solution which requires a huge number of layers in the vertical direction [11].

An alternative form of the three-dimensional equations of motion can be obtained by transforming the complex computational domain, which represents the complex physical geometry, in a regular domain. Such transformation can involve curvilinear coordinate systems which are time-dependent and moves with the free surface: the free surface and the bottom turn out always to be located respectively at the upper and the lower boundary of the computational domain. Moreover, the fluid pressure at the free surface is precisely set to zero, so that no approximation is involved in the assignation of the pressure condition at the upper boundary. In the work of Thomas and Lombard [18], the flow variables are represented by the Cartesian based velocity components multiplied by the Jacobian of the transformation.

The main difficulty in the simulation of the wave propagation from deep to shallow water (including the surf zone) is related to the approach adopted in order to reproduce the wave breaking. In this regard, an approach can be used based on the consideration that the wave breaking can be represented by the discontinuity of the weak solution of the integral form of the motion equations. Weak solution with discontinuity can be obtained by using the integral form of the fluid motion equations expressed in terms of conserved variable (H and $H\overline{v}$, where H is the local depth and $\overline{v}$ is the depth-averaged horizontal velocity), whereas it can't be obtained by using the differential form expressed in function of the primitive variable (H and $\overline{v}$). Furthermore, if shocks are present in the solution, shock waves with erroneous propagation celerity arise in the solution of the differential form of the motion equations expressed in terms of primitive variables. This also happens in the case in which primitive variables are used in a conservative finite-volume scheme that is applied to differential equations in which the convective terms are expressed in divergence form. The integral form of the motion equations, expressed in terms of conserved variables, allow high order shock-capturing numerical schemes to converge to correct weak solutions and, consequently, permit to directly simulate the

breaking of the wave and the energy dissipation associated with it. In literature ([1], [2], [3], [9], [17]), the motion equations are expressed in integral or differential conservative forms and in terms of conserved variables.

In the context defined by the simulation of free surface flows performed by using the motion equations in three-dimensional form integrated by methods of shock-capturing type, Weighted Essentially Non-Oscillatory (WENO) ([5], [12], [14], [7]) are often used, in which the numerical flux is approximated by using a convex combination of all candidate stencils. Reference [14] proposed the cell-averaged version of the WENO scheme where a procedure by which the point values are reconstructed from the cell-averaged values is introduced. The WENO technique uses a combination of low-order reconstructions in order to obtain a higher order approximation. The coefficients which appear in this combination are called linear weights and depends on the local geometry of the meshes. When meshes are uniform or smoothly-varying the linear weights sign is positive, otherwise weights with a negative sign can arise as a consequence of a high degree of mesh irregularity. A monotone scheme cannot be performed by using weights with a negative sign in WENO reconstructions. In order to overcome the limitations of the WENO scheme related to negative linear weight on unstructured grids, remove the dependence of the linear weights on the mesh variability and obtain symmetry conditions, the motion equation numerical solutions can be performed on a time-dependent generalized curvilinear boundary-conforming grid. By following this approach, the domain is turned into a rectangular region which is fixed in time and the fluid variables are directly reconstructed within a modified space in which the grid spacing is constant, so that the regularity of the domain is greatly improved: as a consequence, the linear weights are positive and symmetrical and the monotonicity of the scheme is guaranteed.

In this work, wave transformation is simulated by numerically solving the fluid motion equations written in a new integral form on a coordinate system in which the vertical coordinate is varying in time. The boundary conditions for pressure are placed on the upper face of each computational cell. The solution is advanced in time by using a three-stage Strong Stability Preserving Runge-Kutta (SSPRK) fractional step numerical method which is accurate to the third order, and at each stage a pressure correction formulation is applied in order to get a fluid velocity field which is divergence-free. A shock-capturing technique based on high-order WENO reconstructions is employed in order to discretize the fluid motion equations. At every cell interface, the numerical flux is computed by solving an approximate HLL Riemann problem.

2 The Motion Equations In Time-Dependent Curvilinear Coordinate Systems

In integral form, the continuity and the momentum equations over a control volume $\Delta V(t)$ which varies in time read

$$\frac{d}{dt} \int_{\Delta V(t)} \rho \, dV + \int_{\Delta A(t)} \rho (u_m - v_m) n_m \, dA = 0 \quad (1)$$

$$\frac{d}{dt} \int_{\Delta V(t)} \rho u_l \, dV + \int_{\Delta A(t)} \rho u_l (u_m - v_m) n_m \, dA =$$

$$\int_{\Delta V(t)} \rho f_l \, dV + \int_{\Delta A(t)} T_{lm} n_m \, dA \quad (2)$$

in which $\Delta A(t)$ is the control volume surface, u_l (l=1,3) and v_m (m=1,3) are respectively the velocity of the fluid and the velocity of the control volume surface, both defined in the Cartesian reference coordinate system x^l (l=1,3) (in the present notation it is intended that the superscripts designate components instead of powers), n_m (m=1,3) is the outward unit vector normal to the surface $\Delta A(t)$, ρ is the fluid density, T_{lm} is the stress tensor and f_l (l=1,3) is the vector representing the unit mass body forces

$$f_l = -\frac{1}{\rho} p_{,l} - G \delta_{13} \quad (3)$$

where δ_{13} is the Kronecker delta and p is the total pressure (here the comma with an index in subscript denotes the derivative as $[\ \ ]_{,l} = \partial [\ \ ]/\partial x^l$). The total pressure is defined as the sum of its hydrostatic and dynamic components

$$p = \rho G (\eta - x^3) + q \quad (4)$$

in which G is the gravity constant, η is the elevation of the free surface and q is the dynamic pressure.

It is possible to rewrite the first integral on the right-hand side of (2) in the following way

$$\int_{\Delta V(t)} \rho f_l \, dV = -\int_{\Delta V(t)} [(\rho G \eta + q)_{,l}] \, dV \quad (5)$$

The application of the Green's theorem makes it possible to rewrite the integral on the right-hand side of (5) as follows

$$-\int_{\Delta V(t)}[(\rho G\eta + q)_{,l}]dV =$$

$$-\int_{\Delta A(t)}\rho G\eta n_l dA - \int_{\Delta V(t)}[q_{,l}]dV$$

$$\tag{6}$$

The introduction of (6) into (2) allows us to obtain

$$\frac{d}{dt}\int_{\Delta V(t)}\rho u_l dV =$$

$$-\int_{\Delta A(t)}[\rho u_l(u_m - v_m)n_m + \rho G\eta n_l]dA$$

$$-\int_{\Delta V(t)}[q_{,l}]dV + \int_{\Delta A(t)}T_{lm}n_m dA \tag{7}$$

Equation (7), in which the only external body force is given by the gravitational force, becomes in the case of an incompressible fluid

$$\frac{d}{dt}\int_{\Delta V(t)}\rho u_l dV =$$

$$-\int_{\Delta A(t)}[u_l(u_m - v_m)n_m + G\eta n_l]dA$$

$$-\frac{1}{\rho}\int_{\Delta V(t)}[q_{,l}]dV + \frac{1}{\rho}\int_{\Delta A(t)}T_{lm}n_m dA \tag{8}$$

The first, the second and the third integral on the right-hand side of (8) are respectively related to the convective term and the gradient of the hydrostatic pressure, the gradient of the dynamic pressure and the stress tensor.

For the purpose of simulating the fully dispersive wave phenomena, (8) can be transformed as follows. Let $H(x^1, x^2, t) = h(x^1, x^2, t) + \eta(x^1, x^2, t)$ being h the still water depth. We aim to represent the geometry of the free surface and the bottom in an accurate way and to correctly assign on them the pressure and the kinematic conditions. Let $(\xi^1, \xi^2, \xi^3, \tau)$ be a curvilinear coordinate system which varies in time so as to follow the time variation of the free surface elevation; the following relations define the transformation from the Cartesian coordinates (x^1, x^2, x^3, t) to the curvilinear coordinates $(\xi^1, \xi^2, \xi^3, \tau)$

$$\xi^1 = x^1 \quad \xi^2 = x^2 \quad \xi^3 = \frac{x^3 + h}{H} \quad \tau = t \tag{9}$$

The following relation is also valid

$$v_3 = \frac{\partial x^3}{\partial \tau} \tag{10}$$

Basically, the coordinate transformation described by (9) is such that the time-dependent coordinates of the physical domain are mapped to a uniform transformed space where ξ^3 spans from 0 to 1.

Let $\vec{g}_{(l)} = \partial\vec{x}/\partial\xi^l$ and $\vec{g}^{(l)} = \partial\xi^l/\partial\vec{x}$ be respectively the covariant and the contravariant base vectors. The metric tensor is defined by $g_{(lm)} = \vec{g}_{(l)} \cdot \vec{g}_{(m)}$ and its inverse by $g^{(lm)} = \vec{g}^{(l)} \cdot \vec{g}^{(m)}$ ($l, m = 1,3$) [19]. The Jacobian of the transformation is given by $\sqrt{g} = \sqrt{det(g_{(lm)})}$. The transformation relations between vector $\vec{n}$ expressed in the Cartesian coordinate system and its contravariant and covariant components, $r^{(l)}$ and $r_{(l)}$, expressed in the curvilinear coordinate system are

$$r^{(l)} = \vec{g}^{(l)} \cdot \vec{n} \quad , \quad \vec{n} = r^{(l)}\vec{g}_{(l)}$$

$$r_{(l)} = \vec{g}_{(l)} \cdot \vec{n} \quad , \quad \vec{n} = r_{(l)}\vec{g}^{(l)} \tag{11}$$

These relations also apply to other vectors. It is not difficult to verify that, in the particular case of the above-mentioned transformation, $\sqrt{g} = H$.

We now introduce a restrictive condition on the control volume $\Delta V(t)$: in the following $\Delta V(t)$ must be considered as a volume element defined by surface elements bounded by curves lying on the coordinate lines. Let dA^α be the coordinate surface element on which the coordinate line ξ^α is constant, and $\vec{n}$ the unit vector defined in the Cartesian system of reference normal to the above surface element. Let us indicate with n_m and $g_m^{(\alpha)}$ respectively the m-th component (in the Cartesian reference system) of the unit vector $\vec{n}$ and the covariant base vector $\vec{g}^{(\alpha)}$. We have

$$n_m dA^\alpha = g_m^{(\alpha)}Hd\xi^\beta d\xi^\gamma \tag{12}$$

Let us define the volume element in the physical space as $\Delta V(t) = \Delta x^1\Delta x^2\Delta x^3 = \sqrt{g}\Delta\xi^1\Delta\xi^2\Delta\xi^3$, and the volume element in the transformed space as $\Delta V^* = \Delta\xi^1\Delta\xi^2\Delta\xi^3$. It is not difficult to verify that the first one varies in time, whilst the second one is fixed in time. Similarly to what just made, it is possible to define the surface element in the physical and the transformed space respectively as $\Delta A(t) = \Delta x^\alpha\Delta x^\beta = \sqrt{g}\Delta\xi^\alpha\Delta\xi^\beta$ and $\Delta A^* = \Delta\xi^\alpha\Delta\xi^\beta$ (where $\alpha, \beta = 1, 2, 3$ are cyclic).

Let us also define the cell-averaged value of the primitive variables in the transformed space as

$$\overline{H} = \frac{1}{\Delta V^*}\int_{\Delta V^*}Hd\xi^1 d\xi^2 d\xi^3$$

Giovanni Cannata, Chiara Petrelli, Luca Barsi, Flaminia Camilli, Francesco Gallerano

$$\overline{u}_l = \frac{1}{\Delta V^*} \int_{\Delta V^*} u_l d\xi^1 d\xi^2 d\xi^3 \qquad (13)$$

and the cell-averaged value of the conserved variable as

$$\overline{Hu_l} = \frac{1}{\Delta V^*} \int_{\Delta V^*} Hu_l d\xi^1 d\xi^2 d\xi^3 \qquad (14)$$

By using (9), (12), (13) and (14), (8) becomes

$$\frac{\partial \overline{Hu_l}}{\partial \tau} = \frac{1}{\Delta V^*} \left(-\sum_{\alpha=1}^{3} \left\{ \iint_{\Delta A^{*\alpha+}} [Hu_l(u_m - v_m)g_m^{(\alpha)} \right. \right.$$
$$+ GH^2 g_l^{(\alpha)}] d\xi^\beta d\xi^\gamma - \int_{\Delta A^{*\alpha-}} [Hu_l(u_m$$
$$- v_m)g_m^{(\alpha)} + GH^2 g_l^{(\alpha)}] d\xi^\beta d\xi^\gamma \right\}$$
$$+ \sum_{\alpha=1}^{3} \left\{ \int_{\Delta A^{*\alpha+}} GhH g_l^{(\alpha)} d\xi^\beta d\xi^\gamma \right.$$
$$\left. - \int_{\Delta A^{*\alpha-}} GhH g_l^{(\alpha)} d\xi^\beta d \right\}$$
$$- \frac{1}{\rho} \int_{\Delta V^*} \frac{\partial q}{\partial \xi^k} g_l^{(k)} H d\xi^1 d\xi^2 d\xi^3$$
$$+ \sum_{\alpha=1}^{3} \frac{1}{\rho} \int_{\Delta A^{*\alpha+}} \left\{ T_{lm} g_m^{(\alpha)} H d\xi^\beta d\xi^\gamma \right.$$
$$\left. \left. - \int_{\Delta A^{*\alpha-}} T_{lm} g_m^{(\alpha)} H d\xi^\beta d\xi^\gamma \right) \right.$$
$$\qquad (15)$$

where $\Delta A^{*\alpha+}$ and $\Delta A^{*\alpha-}$ indicate the contour surfaces of the volume element on which ξ^α is constant and which are respectively located at the larger and the smaller value of ξ^α (here the indexes α, β and γ are cyclic). Equation (15) represents the integral form of the momentum equation, expressed in the time-dependent coordinate system $(\xi^1, \xi^2, \xi^3, \tau)$, with the velocities u_l and v_m defined in the Cartesian reference system. Since the integral on the left-hand side of (8) depends on $(\xi^1, \xi^2, \xi^3, \tau)$, the related total time derivative has become a local time derivative in (15). It can be noticed that the conserved variables are advanced in time within a transformed space which is not time-varying. The time variation of the geometric components is expressed by the time variation of the metric terms.

If the density ρ is uniform and constant, (1) changes into

$$\frac{d}{d\tau} \int_{\Delta V^*} H d\xi^1 d\xi^2 d\xi^3 +$$

$$\sum_{\alpha=1}^{3} \left\{ \int_{\Delta A^{*\alpha+}} H(u_m - v_m)g_m^{(\alpha)} d\xi^\beta d\xi^\gamma \right.$$

$$\left. - \int_{\Delta A^{*\alpha-}} H(u_m - v_m)g_m^{(\alpha)} d\xi^\beta d\xi^\gamma \right\} = 0 \qquad (16)$$

which, by making explicit the summation over the index α, reads

$$\frac{d}{d\tau} \int_{\Delta V^*} H d\xi^1 d\xi^2 d\xi^3 +$$

$$\left\{ \int_0^1 \left[\int_{\xi^{1+}} Hu_1 d\xi^2 \right] d\xi^3 - \int_0^1 \left[\int_{\xi^{1-}} Hu_1 d\xi^2 \right] d\xi^3 \right\}$$

$$+ \left\{ \int_0^1 \left[\int_{\xi^{2+}} Hu_2 d\xi^1 \right] d\xi^3 - \int_0^1 \left[\int_{\xi^{2-}} Hu_2 d\xi^1 \right] d\xi^3 \right\}$$

$$+ \left\{ \iint_{\Delta A_{xy}^* (\xi^3=1)} (u_m - v_m)g_m^{(3)} H d\xi^1 d\xi^2 \right.$$

$$\left. - \iint_{\Delta A_{xy}^* (\xi^3=0)} (u_m - v_m)g_m^{(3)} H d\xi^1 d\xi^2 \right\} = 0 \qquad (17)$$

where $\Delta A_{xy}^* = \Delta \xi^1 \Delta \xi^2$ is the horizontal surface element in the transformed space. If the surface and bottom kinematics boundary conditions are taken into account, the last bracket of (17) vanishes. Furthermore, since ΔV^* is not time-varying and H does not depend on ξ^3 and bearing in mind that ξ^3 spans from 0 to 1, the following relation is valid

$$\frac{d}{d\tau} \int_{\Delta V^*} H d\xi^1 d\xi^2 d\xi^3 = \int_0^1 \left[\int_{\Delta A_{xy}^*} \frac{\partial H}{\partial \tau} d\xi^1 d\xi^2 \right] d\xi^3$$

$$= \int_{\Delta A_{xy}^*} \frac{\partial H}{\partial \tau} d\xi^1 d\xi^2 \qquad (18)$$

It is also possible to write

$$\frac{\partial \overline{H}}{\partial \tau} = \frac{1}{\Delta A_{xy}^*} \int_{\Delta A_{xy}^*} \frac{\partial H}{\partial \tau} d\xi^1 d\xi^2 \qquad (19)$$

By applying the bottom and surface kinematic boundary conditions, by using (13), (18) and (19) and by dividing (17) by ΔA_{xy}^*, the following relation is obtained

$$\frac{\partial \overline{H}}{\partial \tau} + \frac{1}{\Delta A_{xy}^*} \int_0^1 \sum_{\alpha=1}^{2} \left[\int_{\xi^{\alpha+}} Hu_\alpha d\xi^\beta \right.$$

$$\left. - \int_{\xi^{\alpha-}} Hu_\alpha d\xi^\beta \right] d\xi^3 = 0$$

$$\qquad (20)$$

in which $\xi^{\alpha+}$ and $\xi^{\alpha-}$ indicate the contour lines of the surface element ΔA^* on which ξ^α is constant and which are located at the larger and at the smaller value of ξ^α respectively. Equation (20) represents the equation which governs the motion of the free surface. Equations (15) and (20) represent the expressions of the three-dimensional equations

of motion as a function of the $\overline{Hu_l}$ and $\overline{H}$ variables in the time-dependent coordinate system $(\xi^1, \xi^2, \xi^3, \tau)$. The simulation of the fully dispersive wave phenomena can be performed by numerically solving (15) and (20). The Smagorinsky sub grid model is used in order to estimate the eddy viscosity in the stress tensor.

3 Numerical Scheme

Equations (15) and (20) are discretized by means of a combined finite-volume and finite-difference scheme with a Godunov-type method. A grid staggering is used where the fluid velocities are located at the centers of the computational cells and the fluid pressure is defined in correspondence of the horizontal faces of the cells. The discretization of the computational domain is based on a grid defined by the coordinate lines ξ^1, ξ^2 and ξ^3 and by the points of coordinates $\xi^1 = j\Delta\xi^1$, $\xi^2 = j\Delta\xi^2$ and $\xi^3 = j\Delta\xi^3$, which represent the centers of the calculation cells $I_{i,j,k} = \left(\xi^1_{i-1/2}, \xi^1_{i-1/2}\right) \times \left(\xi^2_{j-1/2}, \xi^2_{j-1/2}\right) \times \left(\xi^3_{k-1/2}, \xi^3_{k-1/2}\right)$. The state of the system is known at the computational cells center and is identified by the cell-averaged values $\overline{Hu_l}$ and $\overline{H}$. The time level at which the variables are known is $\tau^{(n)}$, whilst the time level at which the variables are unknown is $\tau^{(n+1)}$.

A three-stage Strong Stability Preserving Runge-Kutta (SSPRK) scheme is used in order to solve (15) and (20). With the purpose of getting a fluid velocity field which is divergence-free, a pressure correction formulation is adopted. Once $\overline{Hu_l}^{(n)}$ is known, the following three-stage iteration procedure is implemented in order to compute $\overline{Hu_l}^{(n+1)}$. Let

$$\overline{Hu_l}^{(0)} = \overline{Hu_l}^{(n)} \tag{21}$$

At every stage p (where $p = 1,2,3$), an auxiliary field $\overline{Hu_{l*}}^{(p)}$ is directly computed from (15) by using the values obtained at the previous stage

$$\overline{Hu_{l*}}^{(p)} =$$

$$\sum_{q=0}^{p-1}\left\{\Omega_{pq}\overline{Hu_l}^{(q)} + \Delta\tau\varphi_{pq} D\left[Hu_l^{(q)}, \tau^{(n)} + d_q\Delta\tau\right]\right\} \tag{22}$$

having indicated by $D(H, u_l, \tau)$ the right-hand side of (15) devoid of the dynamic pressure gradient term. Further details on the calculation of coefficients Ω_{pq}, φ_{pq} and d_q can be found in [10]. The continuity equation is not satisfied by the auxiliary fluid

velocity field $\overline{u}_{l*}^{(p)}$ (which is related to the auxiliary variable $\overline{Hu_{l*}}^{(p)}$ computed by (22) starting from the value $\overline{H_*}^{(p-1)}$). For this reason, at every intermediate stage p the fluid velocity field and the fluid pressure field are corrected by means of a scalar potential ψ which is computed by solving the well-known Poisson pressure equation. The latter equation reads as follows

$$\nabla^2\psi^{(p)} = -\frac{\rho}{\Delta t}\nabla\left(\overline{u}_{l*}^{(p)}\right) \tag{23}$$

The irrotational corrector fluid velocity field is calculated by

$$\overline{u}_{1c}^{(p)} = \frac{\Delta t}{\rho}\left(\frac{\partial\psi^{(p)}}{\partial\xi^1} + \frac{\partial\psi^{(p)}}{\partial\xi^3}\frac{\partial\xi^3}{\partial x}\right)$$

$$\overline{u}_{2c}^{(p)} = \frac{\Delta t}{\rho}\left(\frac{\partial\psi^{(p)}}{\partial\xi^2} + \frac{\partial\psi^{(p)}}{\partial\xi^3}\frac{\partial\xi^3}{\partial y}\right)$$

$$\overline{u}_{3c}^{(p)} = \frac{\Delta t}{\rho}\left(\frac{\partial\psi^{(p)}}{\partial\xi^3}\frac{\partial\xi^3}{\partial z}\right) \tag{24}$$

With the purpose of obtaining a non-hydrostatic, divergence-free fluid velocity field at every stage, the fluid velocity field itself has to be corrected in the following way

$$\overline{u}_l^{(p)} = \overline{u}_{l*}^{(p)} + \overline{u}_{lc}^{(p)} \tag{25}$$

Let us indicate with $L(H, u_l, \tau)$ the right-hand side of (20). The depth $\overline{H}^{(p)}$ is advanced at the stage p as follows

$$\overline{H}^{(p)} = \overline{H}^{(p-1)} + L\left(\overline{H}^{(p-1)}, \overline{u}_l^{(p-1)}, \tau^n + \Delta\tau\right) \tag{26}$$

The value of $\overline{Hu_l}^{(n+1)}$ is given by

$$\overline{Hu_l}^{(n+1)} = \overline{Hu_l}^{(3)} \tag{27}$$

In order to calculate the terms $D(H, u_l, \tau)$ and $L(H, u_l, \tau)$, the integrals on the right-hand side of (15) and (20) are numerically approximated. The following sequence is implemented in order to perform the above calculation.

1) At the center of the contour face which is common to two adjacent cells, two point values of the unknown variables are reconstructed by means of two WENO reconstruction defined on the two adjacent cells [6], starting from the cell averaged values.

2) The unknown variables at the contour faces center are advanced in time by means of the solution of

the HLL Riemann problem, in which the initial data are given by the above-mentioned two reconstructed values.

3) The spatial integrals involved in $D(H, u_l, \tau)$ and $L(H, u_l, \tau)$ are calculated by a high-order quadrature rule.

4) The Poisson pressure equation is solved by means of a four-color Zebra line Gauss-Seidel alternate method in conjunction with a multigrid V-cycle technique.

5) The auxiliary velocity fields $\overline{u}_{l*}$ is corrected by means of the scalar potential ψ.

6) The local total depth is advanced in time by (20) by means of the corrected divergence-free non-hydrostatic velocity field.

3.1 WENO reconstructions

With the purpose of explaining the WENO reconstruction technique implemented in this work, let us indicate by $(\overline{u}_l)_{i,j,k}$ the cell averaged values of the Cartesian velocity component u_l over the cell $I_{i,j,k}$. We also indicate by $(u)_{i+1/2,j,k}$ and $(u)_{i-1/2,j,k}$, respectively, the two point values of u_l at the center of the faces over which the coordinate ξ^1 is constant and that are placed on the side of increasing and decreasing ξ^1 (an analogous notation is used the other cell faces). For the sake of brevity, we will only present the reconstruction technique of these point values. Three different steps are involved in this reconstruction:

- Step 1: Starting from the cell averages $(\overline{u}_l)_{i,j,k}$, reconstruction, along the coordinate ξ^3, of the surface averages $(\tilde{u}_l)_{i,j,k}$, that is defined by

$$(\tilde{u}_l)_{i,j,k} = \frac{1}{\Delta\xi^2} \int_{\xi^2_{i-1/2}}^{\xi^2_{i-1/2}} \left[\frac{1}{\Delta\xi^1} \int_{\xi^1_{i-1/2}}^{\xi^1_{i-1/2}} u_l(\xi^1, \xi^2, \xi^3) d\xi^1 \right] d\xi^2 \tag{28}$$

- Step 2: Starting from the surface averages $(\tilde{u}_l)_{i,j,k}$, reconstruction, along the coordinate ξ^2, of the line averages, defined by

$$(\hat{u}_l)_{i,j,k} = \frac{1}{\Delta\xi^1} \int_{\xi^1_{i-1/2}}^{\xi^1_{i-1/2}} u_l(\xi^1, \xi^2, \xi^3) d\xi^1 \tag{29}$$

- Step 3: Starting from the line average $(\hat{u}_l)_{i,j,k}$, reconstruction, along the coordinate ξ^2, of the point values $(u)_{i+1/2,j,k}$ and $(u)_{i-1/2,j,k}$.

1) Step 1

The value of $(\tilde{u}_l)_{i,j,k}$ is reconstructed by using an interpolant polynomial $R_{i,j,k}(\xi^3)$ which is defined in the cell $I_{i,j,k}$ (the subscript i, j, k indicates the cell in which the polynomial is defined) and by using the relation $(\tilde{u}_l)_{i,j,k} = R_{i,j,k}(\xi^3_k)$. According to the formulation of the WENO schemes in the work of [14], the polynomial $R_{i,j,k}(\xi^3)$ is given by a convex combination of three different 2nd order polynomials, $P_{i,j,k+p}(\xi^3) = a_{i,j,k+p}(\xi^3)^2 + b_{i,j,k+p}(\xi^3) + c_{i,j,k+p}$ $(p = -1,0,1)$. The weights of this convex combination are a function of the linear weights and the indexes of smoothness [12]. As suggested in [12], the norm L^2 of the derivatives of the polynomials $P_{i,j,k+p}(\xi^3)$ on cell $I_{i,j,k}$ is used in order to compute the indexes of smoothness. The linear weights are chosen in such a way that the required accuracy is satisfied. The Jacobian terms may affect the weights evaluated in the WENO reconstruction procedure, even when imposing the free stream value. As suggested in [16], the Jacobian terms are not included in the reconstruction procedures and, therefore, the cell averaged value is approximated by

$$(\overline{u}_l)_{i,j,k+p+q} = \frac{1}{\Delta\xi^3} \int_{\xi^3_{k+p+q-1/2}}^{\xi^3_{k+p+q+1/2}} \left\{ \frac{1}{\Delta\xi^2} \right.$$

$$\left. \int_{\xi^2_{j-1/2}}^{\xi^2_{j+1/2}} \left[\frac{1}{\Delta\xi^1} \int_{\xi^1_{i-1/2}}^{\xi^1_{i+1/2}} u_l(\xi^1, \xi^2, \xi^3) d\xi^1 \right] d\xi^2 \right\} d\xi^3 \tag{30}$$

By imposing

$$P_{i,j,k+p}(\xi^3) =$$

$$\frac{1}{\Delta\xi^2} \int_{\xi^2_{j-1/2}}^{\xi^2_{j+1/2}} \left[\frac{1}{\Delta\xi^1} \int_{\xi^1_{i-1/2}}^{\xi^1_{i+1/2}} u_l(\xi^1, \xi^2, \xi^3) d\xi^1 \right] d\xi^2 \tag{31}$$

and by introducing (31) into (30), the above condition becomes

$$(\overline{u}_l)_{i,j,k+p+q} = \frac{1}{\Delta\xi^3} \int_{\xi^3_{k+p+q-1/2}}^{\xi^3_{k+p+q+1/2}} P_{i,j,k+p}(\xi^3) d\xi^3 \tag{32}$$

By introducing the analytical solution of the integral in (32), three independent systems are obtained ($p = -1,0,1$), each of them is formed by three linear equations ($q = -1,0,1$), which permit the computation of the values of the polynomial coefficients $a_{i,j,k+p}$, $b_{i,j,k+p}$, $c_{i,j,k+p}$. Starting from these values and the values of the smoothness indexes, it is possible to calculate $R_{i,j,k}(\xi^3)$ and, consequently, to evaluate $(\tilde{u}_l)_{i,j,k}$.

Giovanni Cannata, Chiara Petrelli, Luca Barsi,
Flaminia Camilli, Francesco Gallerano

2) Step 2

The procedure on which the second step is based is similar to the one illustrated in the previous step. The line averages are reconstructed starting from $(\tilde{u}_l)_{i,j,k}$: this reconstruction is performed along the coordinate ξ^2 and the lines averages are computed by means of the relation

$$(\hat{u}_l)_{i,j,k} = R_{i,j,k}(\xi_j^2) \tag{33}$$

3) Step 3

In the third step, the passages shown in the first step are carried out along the coordinate ξ^1. Starting from the line averages $(\hat{u}_l)_{i,j,k}$, the two point values of the velocity components at the centre of the faces over which the coordinate ξ^1 is constant and that are placed on the side of increasing and decreasing ξ^1 are computed by

$$(u_l)_{i+1/2,j,k} = R_{i,j,k}(\xi^1_{i+1/2})$$

$$(u_l)_{i-1/2,j,k} = R_{i,j,k}(\xi^1_{i-1/2}) \tag{34}$$

3.2 Numerical approximations of the spatial integrals

The numerical approximations of the double and triple integrals on the right-hand side of (15) are obtained by adopting the procedure suggested in [8].

4 Results

In this section, the ability of the proposed model to simulate the vortices formation due to wave-structure interaction is demonstrated by reproducing the experiment carried out by [20] where the passage of a solitary wave over a rigid rectangular submerged obstacle is simulated.

The geometry of the test case consists of a 5m long rectangular channel in which the depth of the still water is $h =$0.228m and a rectangular obstacle of $h/2 =$0.114m high and $L =$0.38m long is located at the bottom (Fig. 1). A grid spacing of 0.0025m, a time step of 0.001s and 100 vertical layers are adopted. The numerical treatment of the obstacle problem is carried out by adopting the strategy proposed by [13]. Since the submerged obstacle brings to a sudden change of the water depth, the elevation of the grid points between the bed and the obstacle top is fixed in time, while between the obstacle top and the free-surface is time-varying in order to follow the water depth modifications. Consequently, the coordinate transformation law expressed by (9) is modified in order to obtain a 2-layer coordinate system.

On the left boundary of the computational domain, the following equations are used in order to generate the solitary wave

$$\eta(t) = A sech^2\left[\sqrt{\frac{3A}{4h^3}}C(t-T)\right] \tag{35}$$

$$u(t) = \frac{C\eta(t)}{h+\eta(t)} \tag{36}$$

where $A =$0.05m is the incident wave amplitude, $C = \sqrt{g(h+A)}$ is the celerity of the wave and $T =$1.0s is the time when the crest of the wave enters the domain.

Two points located behind the rectangular obstacle are considered in order to compare the horizontal and vertical velocities time history between the model results and the experimental data from [20]. The first measurement point (P1) is located 0.034m downstream the rectangular obstacle and 0.040m above the bottom. The second measurement point (P2) is located 0.034m downstream the rectangular obstacle and 0.057m (P2) above the bottom (Fig. 1).
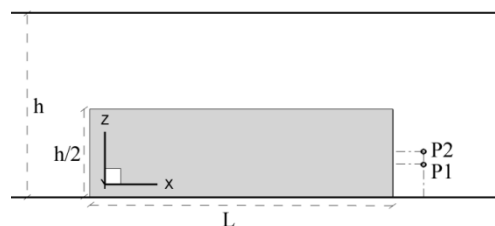

Fig. 1 Dynamics of the vortices generated by the wave-structure interaction. Simulation sketch.

Figures 2 to 6 show the fluid velocity field and the elevation of the free surface due to the wave-submerged obstacle interaction at different instants. As expected, vortical structures are generated both at the left and the right arris of the obstacle, coherently with [13] and [20]. Figure 2 shows that, when the solitary wave approaches the rectangular obstacle, a small vortex is generated on the left corner of the obstacle. In the second of the considered instants (Fig. 3), the passage of the solitary wave produces an increase of the fluid velocity over the whole obstacle. When the peak of the solitary wave has reached the right arris of the rectangular obstacle, a second vortical formation begins to form downstream the obstacle (Fig. 4). As shown in Figures 5 and 6, as the solitary wave propagates over the rectangular obstacle, the vortex formed at the left corner is stretched and the one formed at the right side (downstream the obstacle) grows in strength and size, in accordance with that observed by [13] and [20].

In order to seize the formation and development of the vortex that appears downstream the rectangular obstacle, the time history of the horizontal and

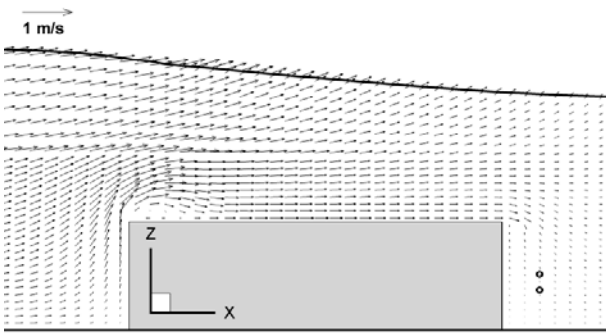vertical velocity components have been registered in the measurement points P1 and P2.

Fig. 2 Dynamics of the vortices generated by the wave-structure interaction. Fluid velocity field and elevation of the free surface at the instant t=2.42s
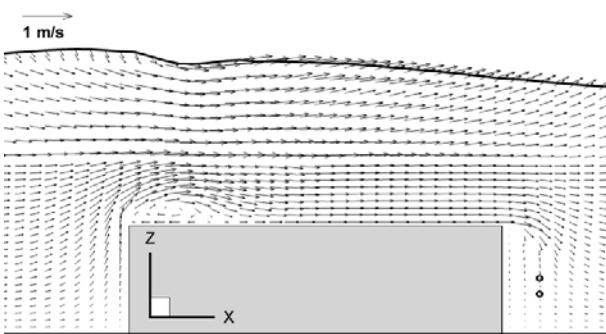

Fig. 3 Dynamics of the vortices generated by the wave-structure interaction. Fluid velocity field and elevation of the free surface at the instant t=2.62s
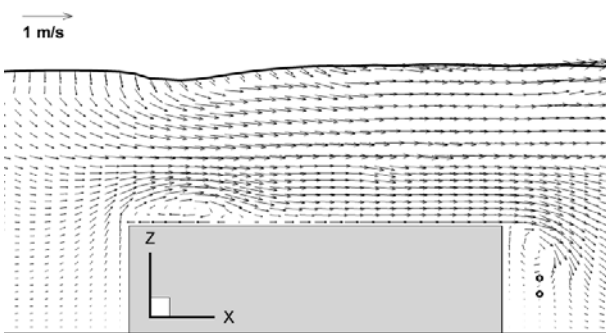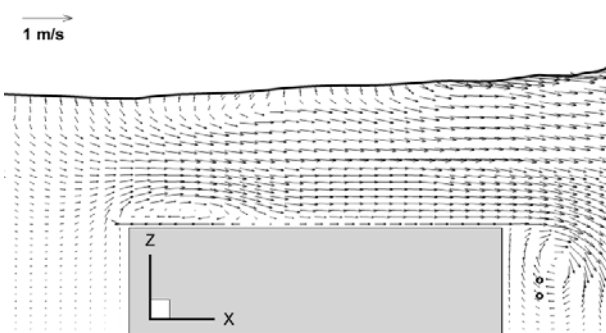

Fig. 4 Dynamics of the vortices generated by the wave-structure interaction. Fluid velocity field and elevation of the free surface at the instant t=2.80s

Fig. 5 Dynamics of the vortices generated by the wave-structure interaction. Fluid velocity field and elevation of the free surface at the instant t=2.98s
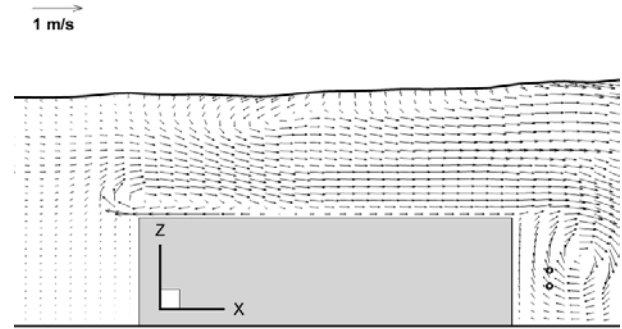

Fig. 6 Dynamics of the vortices generated by the wave-structure interaction. Fluid velocity field and elevation of the free surface at the instant t=3.12s

Figure 7 shows the comparison between the numerical results and the available experimental data from [20] of the dimensionless horizontal velocity ($u_1/\sqrt{gh}$) and dimensionless vertical velocity ($u_3/\sqrt{gh}$) with respect to the real time normalized as $t\sqrt{g/h}$ at the measurement point P1. From this figure, the generation and development of the downstream obstacle vortical motion during the wave-structure interaction can be seen: the horizontal velocity component changes its sign from positive to negative and the vertical velocity component changes its sign from negative to positive.
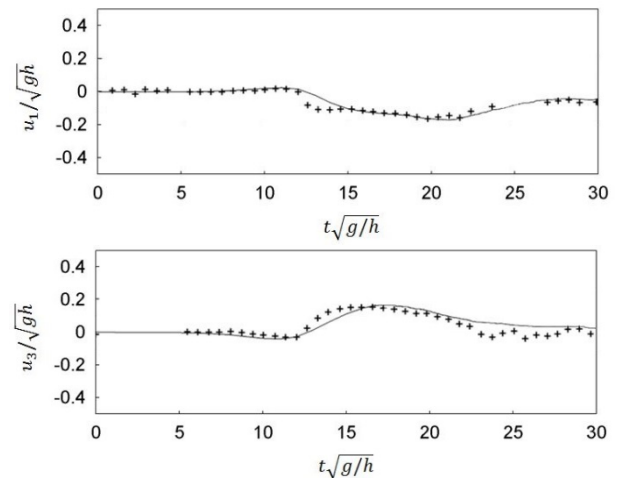

Fig. 7 Dynamics of the vortices generated by the wave-structure interaction. Comparison between the numerical results (solid line) and the experimental data [20] (symbols) of the time history of the dimensionless horizontal ($u_1/\sqrt{gh}$) and vertical ($u_3/\sqrt{gh}$) velocity components at the measurement point P1

Figure 8 shows the comparison between the numerical results and the available experimental data from [20] of the dimensionless horizontal velocity ($u_1/\sqrt{gh}$) and dimensionless vertical velocity ($u_3/\sqrt{gh}$) with respect to the real time normalized as $t\sqrt{g/h}$ at the measurement point P2. Analogously with Figure 7, from Figure 8 it is possible to

recognize the generation and development of the downstream obstacle vortical motion during the wave-structure interaction when the horizontal and vertical velocity components change their signs.

From the differences of the time history of the horizontal and vertical velocity components between the measurement point P1 and P2 (where P2 is placed 0.017m above the measurement point P1) it can be deduced that the vortex formation and its development is a rapidly changing phenomenon.
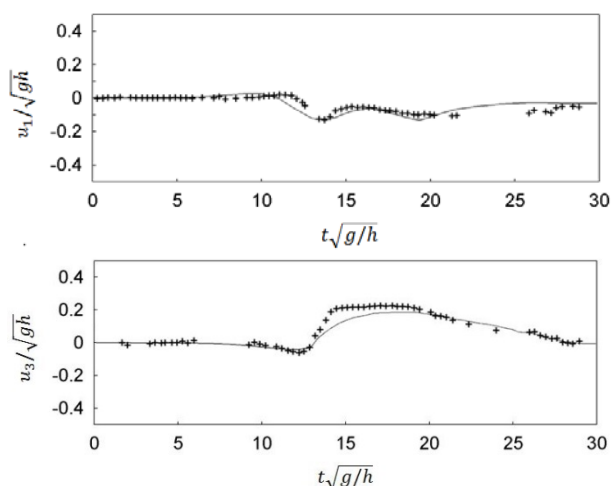

Fig. 8 Dynamics of the vortices generated by the wave-structure interaction. Comparison between the numerical results (solid line) and the experimental data [20] (symbols) of the time history of the dimensionless horizontal ($u_1/\sqrt{gh}$) and vertical ($u_3/\sqrt{gh}$) velocity components at the measurement point P2

From Figures 7 and 8 it can be seen that, at the two measurement points P1 and P2, the time history of both the dimensionless horizontal ($u_1/\sqrt{gh}$) and vertical ($u_3/\sqrt{gh}$) velocity components are in good agreement with the experimental data from [20].

5 Conclusions

A new hydrodynamic model has been proposed which is based on an original integral formulation of the Navier-Stokes equations in a coordinate system in which the vertical coordinate is varying in time. The discretization of the fluid motion equations is performed through a numerical technique which is based on high order WENO reconstructions. The time advancing of the solution is carried out by using a three-stage Strong Stability Preserving Runge-Kutta (SSPRK) fractional step numerical method which is accurate to the third order, and at each stage a pressure correction formulation is applied in order to get a fluid velocity field which is divergence-free. A shock-capturing technique based on high-order WENO reconstructions is employed

in order to discretize the fluid motion equations. At every cell interface, the numerical flux is computed by solving an approximate HLL Riemann problem. As previously demonstrated the new finite-volume non-hydrostatic and shock-capturing three-dimensional model is able to simulate the vortices formation due to wave-structure interaction.

References:
[1] G. Cannata, F. Lasaponara, and F. Gallerano, "Non-Linear Shallow Water Equations numerical integration on curvilinear boundary-conforming grids," WSEAS Transactions on Fluid Mechanics, vol. 10, 2015, pp. 13-25.
[2] G. Cannata, L. Barsi, and F. Gallerano, "Numerical investigation of the coupled flutter onset mechanism for streamlined bridge deck cross-sections," WSEAS Transactions on Fluid Mechanics, vol. 12, 2017, pp. 43-52.
[3] G. Cannata, L. Barsi, and F. Gallerano, "Numerical simulation of the coupled flutter instability for closed-box bridge decks," International Journal of Mechanics, vol. 11, 2017, pp. 128-140.
[4] V. Casulli, and G.S. Stelling, "Numerical simulation of 3D quasi-hydrostatic free surface flows," Journal of Hydraulic Engineering ASCE, vol. 124, 1998, pp. 678-686.
[5] F. Gallerano, and G. Cannata, "Central WENO scheme for the integral form of contravariant shallow-water equations," International Journal for Numerical Methods in Fluids, vol. 67, 2011, pp. 939-959.
[6] F. Gallerano, G. Cannata, and F. Lasaponara, "A new numerical model for simulations of wave transformation, breaking and longshore currents in complex coastal regions," International Journal for Numerical Methods in Fluids, vol. 80, 2016, pp. 571-613.
[7] F. Gallerano, G. Cannata, and F. Lasaponara, "Numerical simulation of wave transformation, breaking run-up by a contravariant fully nonlinear Boussinesq model," Journal of Hydrodynamics B, vol. 28, 2016, pp. 379-388.
[8] F. Gallerano, G. Cannata, and M. Tamburrino, "Upwind WENO scheme for shallow water equations in contravariant formulation," Computers & Fluids, vol. 62, 2012, pp. 1-12.
[9] F. Gallerano, G. Cannata, and M. Villani, "An integral contravariant formulation of the fully nonlinear Boussinesq equations," Coastal Engineering, vol. 83, 2014, pp. 119-136.
[10] S. Gottlieb, D.I. Ketcheson, and C.W. Shu, "High order strong stability preserving time discretization," Journal of Scientific Computing, vol. 38, 2009, pp. 251-289.

Giovanni Cannata, Chiara Petrelli, Luca Barsi,
Flaminia Camilli, Francesco Gallerano

[11] A.A. Issakhov, and G. Mussakulova, "Numerical study for forecasting the dam break flooding flows impacts on different shaped obstacles," International Journal of Mechanics, vol. 11, 2017, pp. 273-280.

[12] G.S. Jiang, and C.W. Shu, "Efficient implementation of weighted ENO schemes," Journal of Computational Physics, vol. 126, 1996, pp. 202-228.

[13] P. Lin, "A multiple layer σ-coordinate model for simulation of wave-structure interaction," Computers & Fluids, vol. 35, 2006, pp. 147-167.

[14] X.D. Liu, S. Osher, and T. Chan, "Weighted essentially non-oscillatory schemes," Journal of Computational Physics, vol. 115, 1994, pp. 200-212.

[15] G. Ma, F. Shi, and J.T. Kirby, "Shock-capturing non-hydrostatic model for fully dispersive surface wave processes," Ocean Modeling, vol. 43-44, 2012, pp. 22-35.

[16] T. Nonomura, N. Iizuka, and K. Fujii, "Free stream and vortex preservation properties of high-order WENO and WCNS on curvilinear grids," Computers & Fluids, vol. 39, 2010, pp. 197-214.

[17] F. Shi, J.T. Kirby, J.C. Harris, J.D. Geiman, and S.T. Grilli, "A high-order adaptive time-stepping TVD solver for Boussinesq modeling of breaking waves and coastal inundation," Coastal Engineering, vol. 43-44, 2012, pp. 36-51.

[18] P.D. Thomas, and C.K. Lombard, "Geometric conservation law and its application to flow computations on moving grids," AIAA Journal, vol. 17, 1979, pp. 1030-1037.

[19] J.F. Thompson, Z.U.A. Warsi, and C.W. Mastin, Numerical grid generation: foundations and applications, Elsevier North-Holland, New York, 1985.

[20] F. Zhuang, and J.J. Lee, "A viscous rotational model for wave overtopping over marine structure," Proceedings of the 25th International Conference of Coastal Engineering, ASCE, 1996, pp.2178-2191.